Geochemistry Geophysics Geosystems G3
AN ELECTRONIC JOURNAL OF THE EARTH SCIENCES
Published by AGU and the Geochemical Society

Article
Volume 8, Number 11
22 November 2007
Q11007, doi:10.1029/2007GC001720
ISSN: 1525-2027

Paleointensity-assisted chronostratigraphy of detrital layers on the Eirik Drift (North Atlantic) since marine isotope stage 11

Helen F. Evans and James E. T. Channell
Department of Geological Sciences, University of Florida, P.O. Box 112120, Gainesville, Florida 32611, USA (geohelen@ufl.edu)

Joseph S. Stoner
College of Oceanic and Atmospheric Sciences (COAS), Oregon State University, 104 COAS Administration Building, Corvallis, Oregon 97331-5503, USA

Claude Hillaire-Marcel
Centre de Recherche en Géochimie et en Géodynamique (GEOTOP), Universitè du Québec à Montreal, C.P. 8888, Succ. Centre-Ville, Montreal, Quebec, Canada H3C 3P8

James D. Wright, Lauren C. Neitzke, and Gregory S. Mountain
Wright Laboratories, Department of Geological Sciences, Rutgers University, Piscataway, New Jersey 08854, USA

[1] Four piston cores collected in 1999 and 2002 from the Eirik Drift (southern Labrador Sea, off SE Greenland) provide paleomagnetic, environmental magnetic, and oxygen isotope records back to marine isotope stage 11. Age models for the cores are based on a combination of planktonic oxygen isotope data, relative geomagnetic paleointensity proxies, and the identification of geomagnetic excursions (Laschamp and Iceland Basin). Environmental magnetic data delineate two distinct detrital signals, interpreted to reflect the behavior of the surrounding ice sheets (Greenland and Laurentide) to orbital- and millennial-scale climate forcing. Broad decimeter-scale intervals of increased magnetic concentration and grain size occur during the early part of interglacial marine isotopic stages (MIS) 1, 5, 7, 9, and 11. Discrete centimeter-scale layers, recognized by magnetic concentration and grain-size sensitive parameters, gamma ray attenuation (GRA) bulk density, and carbonate content, are observed in glacial and interglacial stages as well as during terminations. On the basis of glacial reconstructions on Greenland during the last termination, the broad decimeter-scale coarser-grained intervals can be attributed to detrital influx associated with the retreat of the terrestrial-based Greenland Ice Sheet in the early Holocene. A similar magnetic signal observed within interglacial MIS 5, 7, 9, and 11 indicates similar Greenland Ice Sheet behavior during these time intervals. Two types of centimeter-scale detrital layers are also recognized back to MIS 11. Detrital carbonate (DC) layers reflect predominately ice-rafted debris (IRD) deposition, while the low detrital carbonate (LDC) layers reflect mass movement as evidenced by sharp basal contacts, graded bedding, and traction structures, likely from the Greenland slope. Some detrital layers on Eirik Drift, particularly the DC layers, can be tentatively correlated to detrital layers observed in the central North Atlantic and to those documented on the southern side of the Labrador Sea at Orphan Knoll.

Components: 9734 words, 13 figures, 4 tables.

Keywords: paleointensity.

Index Terms: 1521 Geomagnetism and Paleomagnetism: Paleointensity; 1540 Geomagnetism and Paleomagnetism: Rock and mineral magnetism.

Received 12 June 2007; **Revised** 30 July 2007; **Accepted** 9 August 2007; **Published** 22 November 2007.

Evans, H. F., J. E. T. Channell, J. S. Stoner, C. Hillaire-Marcel, J. D. Wright, L. C. Neitzke, and G. S. Mountain (2007), Paleointensity-assisted chronostratigraphy of detrital layers on the Eirik Drift (North Atlantic) since marine isotope stage 11, *Geochem. Geophys. Geosyst.*, *8*, Q11007, doi:10.1029/2007GC001720.

1. Introduction

[2] The recognition of detrital sedimentation in the North Atlantic as paleoceanographically significant [e.g., *Heinrich*, 1988; *Broecker et al.*, 1992; *Bond et al.*, 1992; *Ruddiman*, 1977] was one of the key observations in the development of current understanding of abrupt climate change [*Alley and MacAyeal*, 1994]. Heinrich layers were originally defined by their high lithic to foraminifer percentage and increased abundance of *N. pachyderma* [*Heinrich*, 1988]. Attributed to massive release of icebergs originating predominantly in the Hudson Strait region, these layers were originally labeled "H1" through "H6" [*Bond et al.*, 1992], and at least eight such layers are now documented during cold stadials of the last glacial cycle recorded in the Greenland Ice Cores [*Bond et al.*, 1993]. In the North Atlantic, four Heinrich layers (H1, H2, H4 and H5) contain high abundance of detrital carbonate [*Bond et al.*, 1992; *Broecker et al.*, 1992] that is sourced from the Hudson Strait region, where the Laurentide Ice Sheet (LIS) was underlain by Paleozoic carbonate rocks [*MacAyeal*, 1993]. H3 and H6 differ from other Heinrich layers and show only a slight increase in flux of lithic grains and low foraminifera percentages, and are thought to contain detrital contributions from European sources (see review by *Hemming* [2004]). Many studies of North Atlantic detrital-layer stratigraphy have been focused on the so-called IRD belt [*Ruddiman*, 1977] of the central North Atlantic [e.g., *Bond et al.*, 1992, 1999; *Grousset et al.*, 1993; *Bond and Lotti*, 1995; *Snoeckx et al.*, 1999], with other studies documenting these layers in more ice-proximal locations such as the Labrador Sea [e.g., *Andrews and Tedesco*, 1992; *Hillaire-Marcel et al.*, 1994; *Stoner et al.*, 1995b, 1996, 2000; *Hiscott et al.*, 2001], the Irminger Basin off east Greenland [*Elliot et al.*, 1998; *van Kreveld et al.*, 2000], and the Porcupine Seabight off SW Ireland [*Scourse et al.*, 2000; *Walden et al.*, 2007; *Peck et al.*, 2007]. In this study, we use the term "detrital layer" to refer to centimeter-scale, rapidly deposited, generally coarse-grained layers with little or no biogenic material, derived from multiple modes of deposition, not necessarily ice rafting.

[3] Correlations of detrital layers across the North Atlantic for the last glacial cycle have been based on radiocarbon ages, and correlations of isotopic data and sea-surface temperature proxies to the Greenland ice core chronologies [e.g., *Bond et al.*, 1999]. Determining the sources of detritus in these layers, and correlating them across the North Atlantic is critical to our understanding of the ice sheet response to climate forcing. Due to the increasing number of detrital layers recognized in ice-proximal locations such as Orphan Knoll [e.g., *Hillaire-Marcel et al.*, 1994], and the short duration of detrital layer deposition, their unequivocal correlation from site to site presents challenges that test the limits of stratigraphic resolution, particularly beyond the range of radiocarbon age dating and Greenland ice core chronologies.

[4] In this paper, we document the detrital layer stratigraphy of the Eirik Drift, off SE Greenland, back to marine isotope stage (MIS) 11, and use a combination of oxygen isotope data and relative paleointensity (RPI) proxies to facilitate correlations to other records. Due to the rate of change of geomagnetic field intensity (~5% per century for the last few centuries), geomagnetic paleointensity records have potential for high-resolution correlation. Their utility depends on the fidelity of the sediment as a geomagnetic recorder, and the accumulation rates of individual records. It has been demonstrated that RPI proxies can be correlated throughout the North Atlantic Ocean [*Channell*, 1999; *Laj et al.*, 2000] to the South Atlantic [*Channell et al.*, 2000; *Stoner et al.*, 2000] and to the Pacific Ocean [*Yamazaki*, 1999; *Horng et al.*,

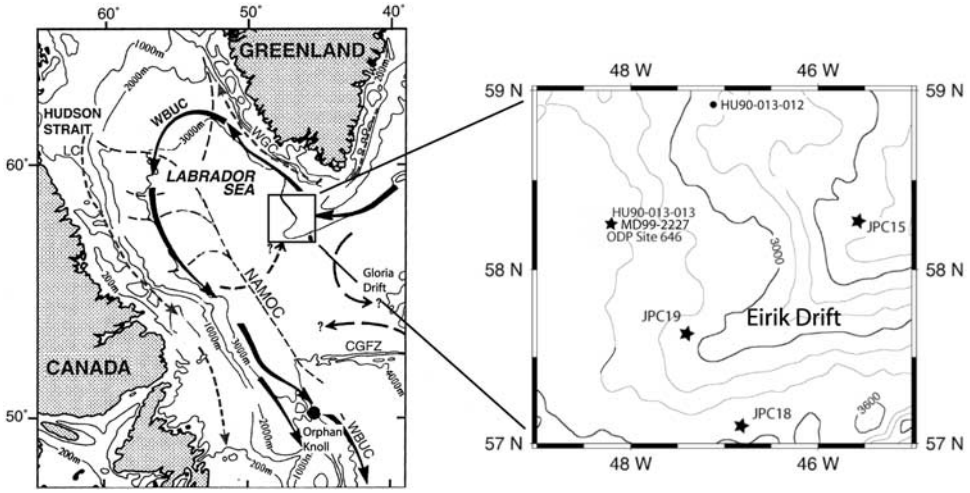

Figure 1. Location map for piston cores JPC15, JPC18, JPC19, and MD99-2227. Arrows indicate the path of the Western Boundary Undercurrent. NAMOC, Northwest Atlantic Mid-Ocean Channel; CGFZ, Charlie Gibbs Fracture Zone. Left-side map modified after *Hillaire-Marcel and Bilodeau* [2000].

2003], and several global paleointensity stacks have been compiled [*Guyodo and Valet*, 1999; *Laj et al.*, 2004].

[5] The Labrador Sea is a climatically sensitive region that was surrounded during the last glacial interval by massive continental ice sheets: the Greenland Ice Sheet and the Laurentide Ice Sheet (LIS). Eirik Drift is a canopy of Pliocene-Quaternary sediments reaching thicknesses of several kilometers that drapes the underlying Eirik Ridge [*McCave and Tucholke*, 1986]. Magnetic anomalies have not been identified directly beneath the Eirik Ridge, although the adjacent oceanic crust in both the Irminger Basin and Labrador Sea is associated with marine magnetic anomaly 24 of Paleocene-Eocene boundary age [*Srivastava and Tapscott*, 1986]. The Eirik Drift is 800 km long and has been constructed by the interaction of the southwestward flowing Western Boundary Undercurrent (WBUC) and basement topography [*Chough and Hesse*, 1985]. The WBUC carries water masses originating from the Norwegian Sea and Greenland seas that enter the North Atlantic over the Iceland-Scotland Ridge and Denmark Strait (Figure 1) [*McCave and Tucholke*, 1986; *Lucotte and Hillaire-Marcel*, 1994]. The WBUC moves over, and constructs, the Eirik Drift and then follows bathymetric contours around the Labrador Basin [*McCave and Tucholke*, 1986].

[6] We present data from three jumbo piston cores (JPC15, JPC18, JPC19) collected on the Eirik Drift in the summer of 2002 during Cruise KN166-14 of the R/V *Knorr*, and from Core MD99-2227 collected during the 1999 *Images* campaign (Figure 1). Core JPC15 was taken on the upper slope of the ridge at a water depth of 2230 m. Core JPC19 was collected from the crest of the ridge at a water depth of 3184 m, and Core JPC18 from the southern flank of the ridge at a water depth of 3435 m. Core MD99-2227 was collected from the western toe of the drift at 3460 m water depth. The recovered sediments are mostly dark gray bioturbated silty clays, with clayey silt and sandy mud, and occasional gray nannofossil/foraminifer rich clayey silt layers (see *Turon et al.* [1999] for a lithologic description of MD99-2227). We identify detrital layers in these cores using magnetic, petrologic and physical property data, and use a combination of relative paleointensity proxies and planktic oxygen isotope records to construct chronologies that facilitate correlation within the North Atlantic region.

2. Prior Regional Studies

[7] Prior studies of sediments from the Eirik Drift have included Ocean Drilling Program (ODP) Site 646 (ODP Leg 105), and piston and gravity cores collected during cruises by the *CSS Hudson* in 1990 and the *Marion Dufresne* in 1999. Seismic records used to extrapolate the sequence recovered at Site 646 indicate that the drift has been constructed since the middle to early Pliocene [*Arthur et al.*, 1989]. Although sedimentation on the drift sequence was more or less continuous during the Late Pliocene and Pleistocene, sedimentation rates vary considerably with glacial/interglacial condi-

Table 1. Latitude, Longitude, Water Depth, Length, and Basal Age of the Studied Cores

Core	Long., °W	Lat., °N	Water Depth, m	Base Age, ka	Core Length, m
JPC15	45.57	58.20	2230	165	23.3
JPC18	47.13	57.19	3435	310	23.7
JPC19	47.60	57.58	3184	250	23.3
MD99-2227	48.22	58.12	3460	430	42.96

tions, and with location on the drift [e.g., *Hillaire-Marcel et al.*, 1994].

[8] The Pleistocene sediments at ODP Site 646 comprise bioturbated silty clays, with numerous centimeter- to decimeter-scale intervals of detrital carbonate silts and thin beds of laminated and cross-laminated siliciclastic sandy-silty mud [*Hiscott et al.*, 1989]. Eleven centimeter-scale detrital carbonate beds (carbonate >50%) were identified in sediments of the last 450 ka; some are characterized by delicate laminae and/or grading, and were interpreted as turbidites [*Hiscott et al.*, 1989]. As the carbonate mineralogy of these layers (a 2:1 calcite-to-dolomite ratio) resembles that of the Northwest Atlantic Mid-Ocean Channel (NAMOC) levee sediments, detrital layers were interpreted as spillover turbidites from the NAMOC [*Hesse et al.*, 1987; *Hiscott et al.*, 1989]. In addition to the carbonate-rich detrital layers, thin beds of laminated and cross-laminated siliciclastic sandy-silty mud were interpreted as contourites deposited during periods of stronger bottom current activity [*Hiscott et al.*, 1989]. Interpretation of the oxygen isotope stratigraphy was compromised by poor recovery at Site 646 [*Aksu et al.*, 1989].

[9] Piston cores HU90-013-012 (water depth: 2830 m) and HU90-013-013 (water depth: 3380 m) (Figure 1), collected in 1990 during a cruise of the *CSS Hudson*, record the last glacial cycle at differing water depths on the Eirik Drift [*Hillaire-Marcel et al.*, 1994]. Core HU90-013-013 shows high sedimentation rates in the Holocene while Core HU90-013-012 is characterized by condensed interglacial sedimentation likely due to its position relative to the WBUC [*Stoner et al.*, 1995a, 1996]. Increases in magnetic concentration and grain size during the early Holocene and at the MIS 6/5e transition in HU90-013-013 were attributed to detrital influx associated with retreat of the Greenland Ice sheet [*Stoner et al.*, 1995b]. Four detrital layers were identified within MIS 2 and 3 in Core HU90-013-013, on the basis of their magnetic properties (coarse magnetic grain size) and relatively high percent carbonate values, and three of these layers were correlated to Heinrich Events 1, 2 and 4 [*Stoner et al.*, 1996, 1998]. The chronology for these cores was based on a combination of relative paleointensity proxies, oxygen isotopes and radiocarbon ages.

[10] *Hillaire-Marcel et al.* [1994] interpreted detrital carbonate (DC) and low detrital carbonate (LDC) layers deposited during the last glacial cycle at Orphan Knoll from core HU91-045-094, on the western side of the Northwest Atlantic Mid-Ocean Channel, as being related to ice advances of the Laurentide Ice Sheet that triggered turbiditic flows down the NAMOC (Figure 1). Sediment suspended by these flows is thought to have deposited centimeter-scale sandy mud beds rich in detrital carbonate (DC layers) at Orphan Knoll. *Stoner et al.* [2000] placed the detrital layer stratigraphy from core MD95-2024 from Orphan Knoll on a GISP2 (Greenland ice core) chronology by correlation of the detrital layers at Orphan Knoll with the cold stadials in the Greenland ice core. Their chronology was consistent with the correlation between the relative paleointensity record from Core MD95-2024 and the ^{10}Be record from the GISP2 ice core [*Stoner et al.*, 2000].

[11] Sediment is supplied to the Eirik Drift via bottom currents that move along the East Greenland margin bringing sediment from the East Greenland shelf and Irminger Basin to the Eirik Drift. *Elliot et al.* [1998] studied Core SU90-42 from the East Greenland Margin (62°40′N 37°22′W), about 350 km upstream along the path of the WBUC, and identified Heinrich layers 1–5 and thirteen other detrital events of smaller amplitude during the last 60 ka. These layers were interpreted as IRD from small-scale iceberg discharges occurring on millennial timescales.

3. Methods

[12] U-channel samples (2 × 2 cm square cross-section and 150 cm in length) were collected from the center of the split face of piston core sections. These samples were measured on a 2G-Enterprises narrow-access pass-through cryogenic magnetometer at the University of Florida. Natural remanent magnetization (NRM) was demagnetized stepwise using alternating fields (AF) in 5 mT increments for 0–60 mT peak fields, and in 10 mT increments

Table 2. Properties of Detrital Carbonate and Low Detrital Carbonate Layers in Core MD99-2227

Event	Thickness, cm	Depth, cm	Age, ka	MIS	Name[a]	k peak	k_{ARM}/k	% Carb	GRAPE Density	% Detrital Carbonate	X-Ray	Sharp Base	Grading	% > 106μm
1	5	440	9.1	1/2	1LDC	yes	coarse	low	peak	10	traction	yes	yes	0.08
2	14	617	20.2	2	2LDC	yes	coarse	low	peak	trace	traction	yes	yes	0.34
3	15	663	22.8	2	2DC	no		high	peak	15		no	no	0.97
4	21	859	39.1	3	3DC	no	coarse	high	peak	40		no	no	3.18
5	6	1872	111.7	5	5LDC	yes	coarse	low	peak	trace		yes	no	3.32
6	16	2019	129.3	5	5DC	no	fine	high	peak	70		no	no	0.42
7	14	2193	152.2	6	6LDC	yes	coarse	low	peak	trace	traction	yes	yes	0.81
8	16	2505	191.6	7	7DCa	yes	coarse	high		20	IRD rich	no	no	7.05
9	12	2700	215	7	7DCb	no		high	peak	25		no	no	0.67
10	6	2872	233.4	7	7LDC	yes	coarse	low	peak	trace	traction	yes	no	0.38
11	11	3084	266.6	8	8DC	no	coarse	high	peak	20	IRD rich	no	no	15.92
12	17	3229	290	9	9DC	no	fine	high	peak	30		no	no	0.24
13	5	3536	335.6	9/10	9LDC	yes	coarse	low	peak	trace	traction	yes	no	0.04
14	18	4008	391	11	11LDCa	yes	coarse	low	peak	trace	traction	yes	no	0.04
15	4	4084	403.5	11	11LDCb	yes	coarse	low	peak	5	traction	yes	yes	1.55
16	7	4134	409.6	11	11LDCc	yes	coarse	low	peak	10	traction	yes	yes	0.03
17	7	4240	421.4	11	11DC	no	coarse	high	peak	50	IRD rich	no	no	21.31

[a]DC, detrital carbonate; LDC, low detrital carbonate.

for 60 mT–100 mT peak fields. Volume susceptibility was then measured using a susceptibility track specifically designed for u-channels [*Thomas et al.*, 2003] that has a measurement resolution of a few centimeters. Anhysteretic remanent magnetization (ARM) was applied using an AF field of 100 mT and a bias DC field of 50 μT. Isothermal remanent magnetization (IRM) was imparted using a 0.5 T DC field. Both artificial remanences were demagnetized with the same AF steps used to demagnetize NRM. Principal components were calculated from the NRM data using the method of *Kirschvink* [1980] applied to the 20–80 mT demagnetization interval. Back-to-back discrete samples (8-cm^{-3} and 1-cm^{-3} cubes) were collected, alongside the u-channel trough, across intervals where magnetic excursions were detected in u-channel data. These discrete samples were stepwise demagnetized using AF, and components calculated using the standard [*Kirschvink*, 1980] method.

[13] Relative paleointensity proxies were generated by normalizing the NRM data by both ARM and IRM, demagnetized at a common peak field. A mean of nine normalized remanence values, in the 20–60 mT peak field range, was used to generate the relative paleointensity proxies. ARM and susceptibility data were also used to ascertain magnetic grain size changes that help define detrital layers. The parameter k_{arm} (anhysteretic susceptibility), obtained by normalizing ARM intensity by the strength of the dc field used to acquire the ARM, was divided by volume susceptibility, to determine k_{arm}/k, a proxy for magnetite grain size.

[14] On completion of the magnetic measurements on the u-channel samples, X-radiographs were taken across detrital layers, identified by u-channel magnetic measurements and carbonate analyses, to provide a picture of the internal structure of these layers and identify the presence or absence of traction structures. Discrete toothpick-sized samples, collected at 1-cm intervals across detrital layers, were used for smear slide observation (Table 2) and for measurement of magnetic hysteresis parameters using a Princeton Measurements Corp. vibrating sample magnetometer (VSM). The samples were placed in small gelatin capsules and fitted to the base of the VSM probe. Magnetic hysteresis parameters provide an additional means of estimating magnetite grain size.

[15] Cores were sub-sampled for oxygen isotope analysis at 5-cm spacing. Samples from Core MD99-2227 were analyzed at GEOTOP (Montreal) while samples from the KN166-14 cores

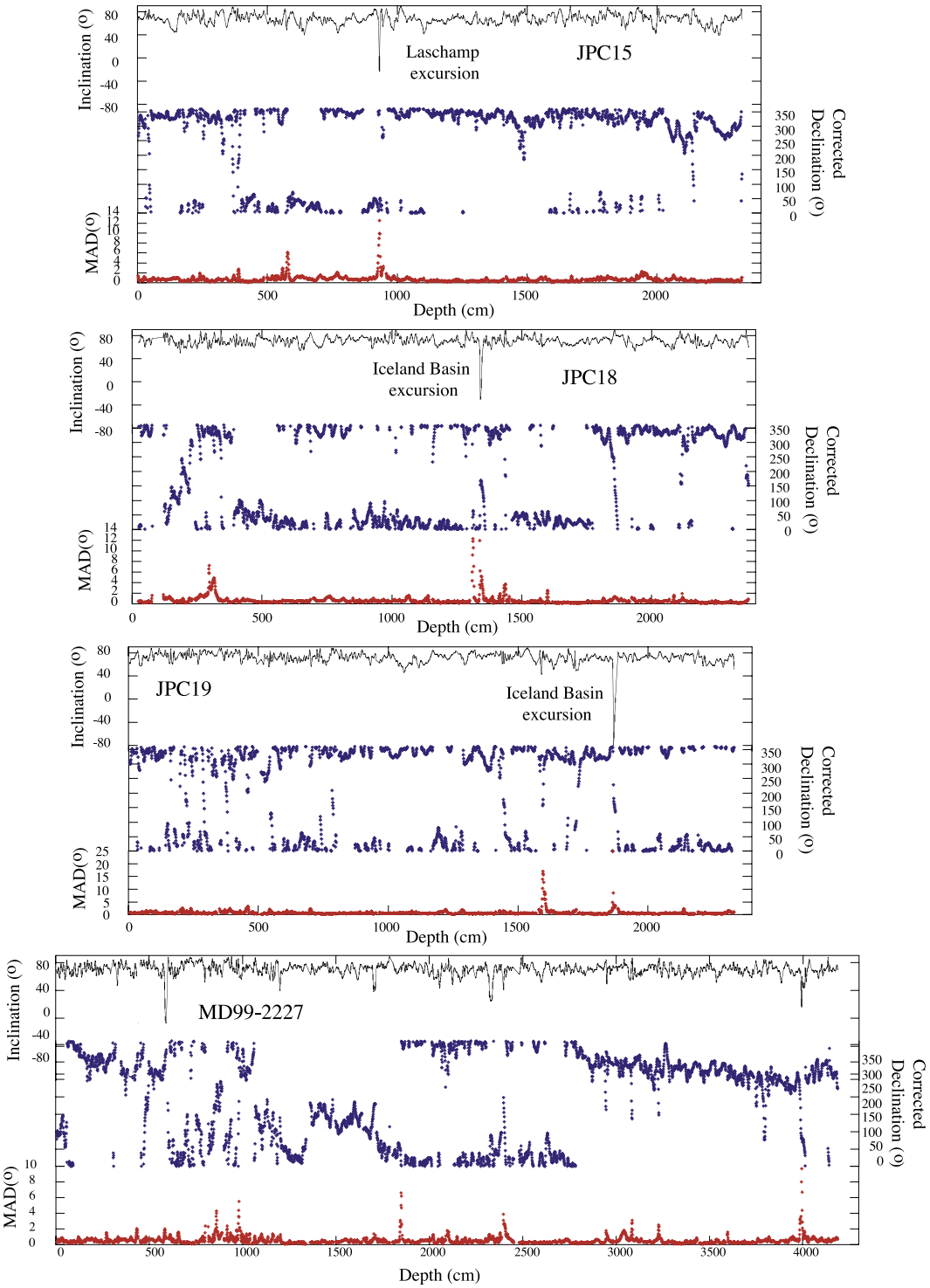

Figure 2. Component inclination, corrected component declination, and maximum angular deviation (MAD) values for Cores JPC15, JPC19, JPC18, and MD99-2227.

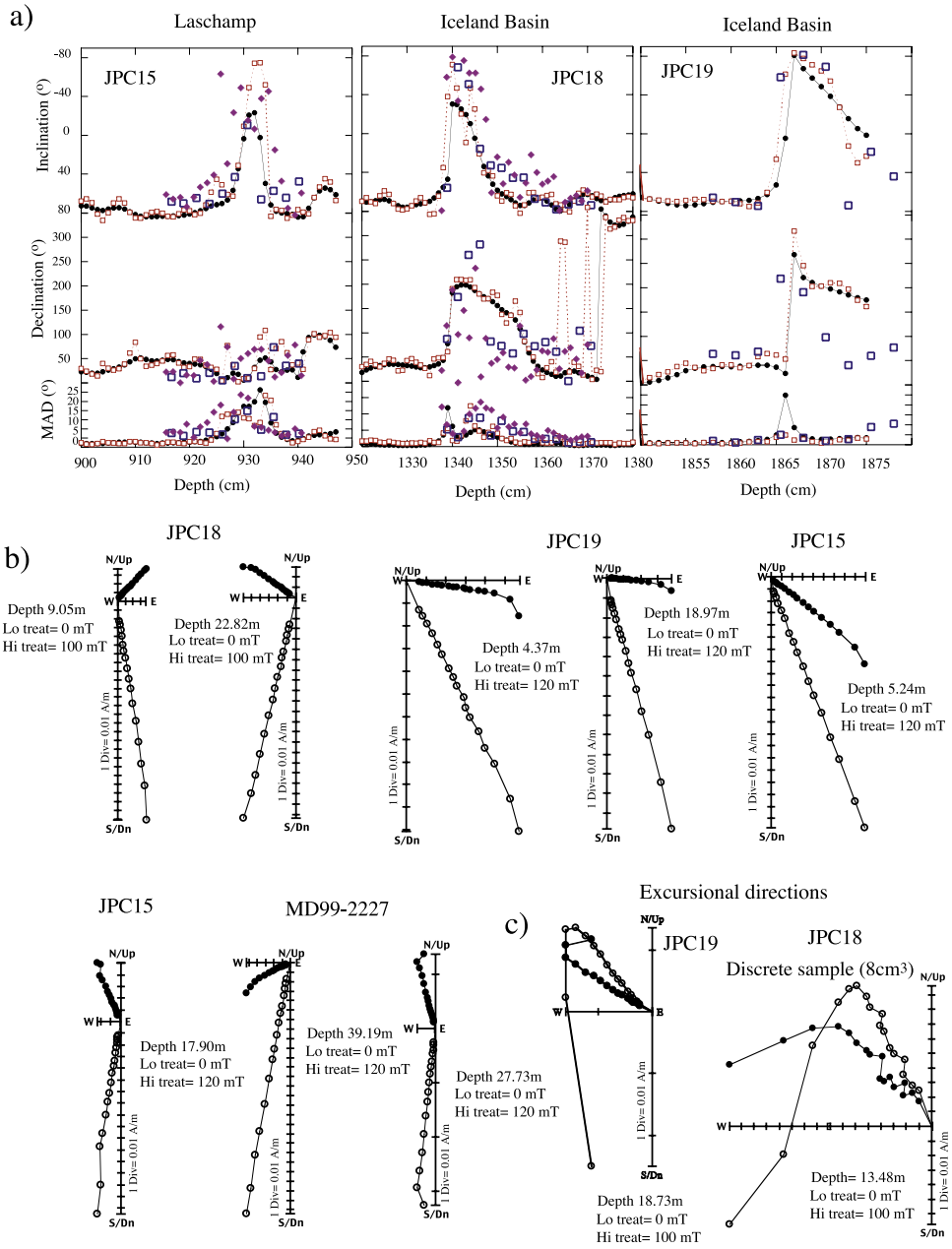

Figure 3. (a) Component inclination, declination, and maximum angular deviation (MAD) values recording Laschamp and Iceland Basin magnetic excursions in piston cores JPC15, JPC18, and JPC19. Key: U-channel data (closed circles), deconvolved u-channel data (open squares-dashed line), 8-cm^3 discrete sample cubes (open squares), and 1-cm^3 cubes (diamonds). (b) Orthogonal projections of alternating field demagnetization data for representative samples from Cores JPC15, JPC18, JPC19, and MD99-2227. Open and closed symbols represent projections on the vertical and horizontal planes, respectively. (c) Orthogonal projections of alternating field demagnetization data showing excursional directions associated with the Iceland Basin excursion from Cores JPC18 and JPC19.

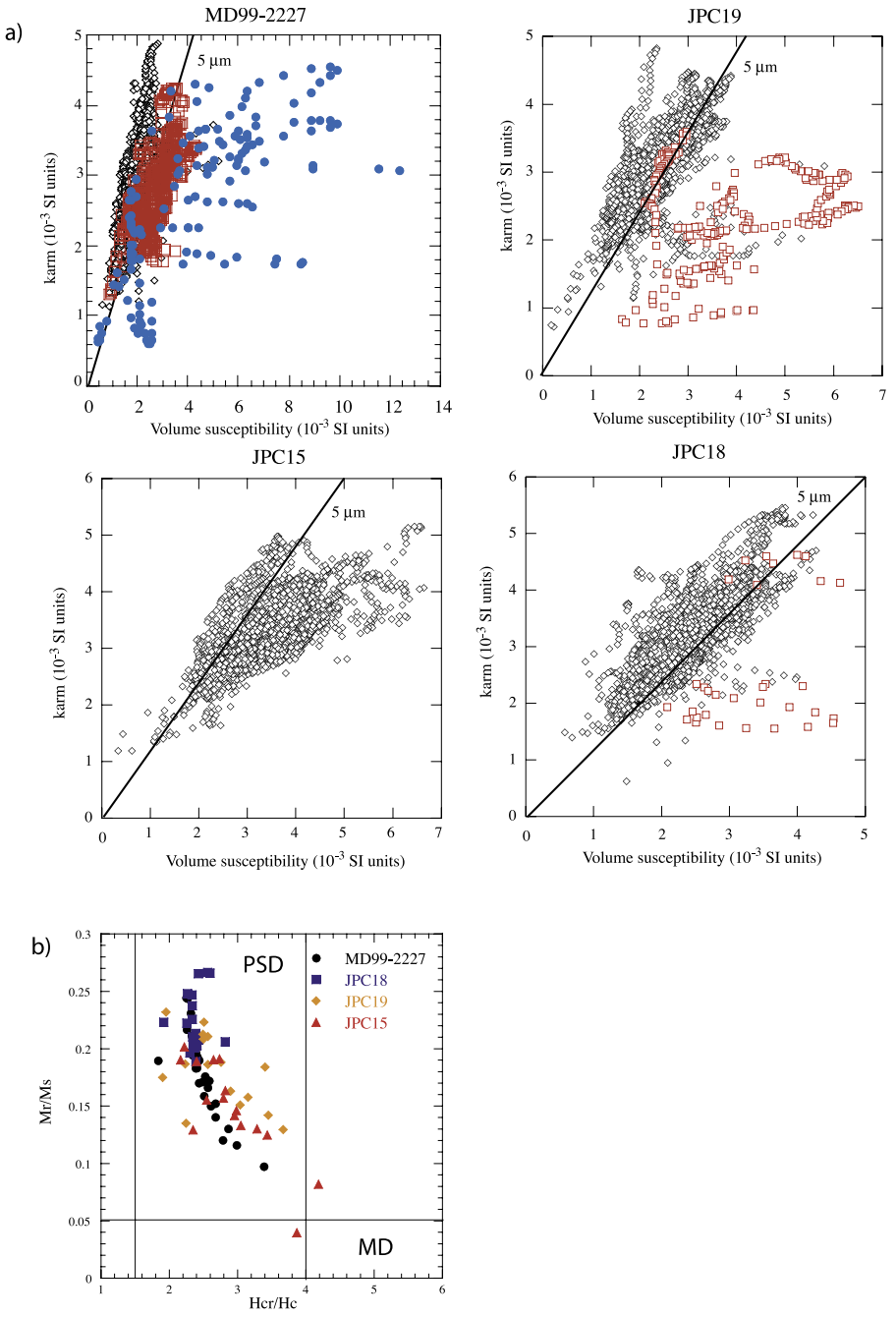

Figure 4. (a) Anhysteretic susceptibility (k_{arm}) plotted against volume susceptibility (k) for Cores JPC18, JPC19, JPC15, and MD99-2227. Diamonds indicate "background" sediment, red squares indicate coarse-grained high-susceptibility intervals at the onset of interglacials, and blue circles indicate centimeter-scale detrital layers. The 5 μm magnetic grain-size line is placed using the calibration of *King et al.* [1983]. (b) Hysteresis ratio plot for Cores JPC15, JPC18, JPC19, and MD99-2227. Pseudo-single domain (PSD) and multidomain (MD) fields after *Day et al.* [1977].

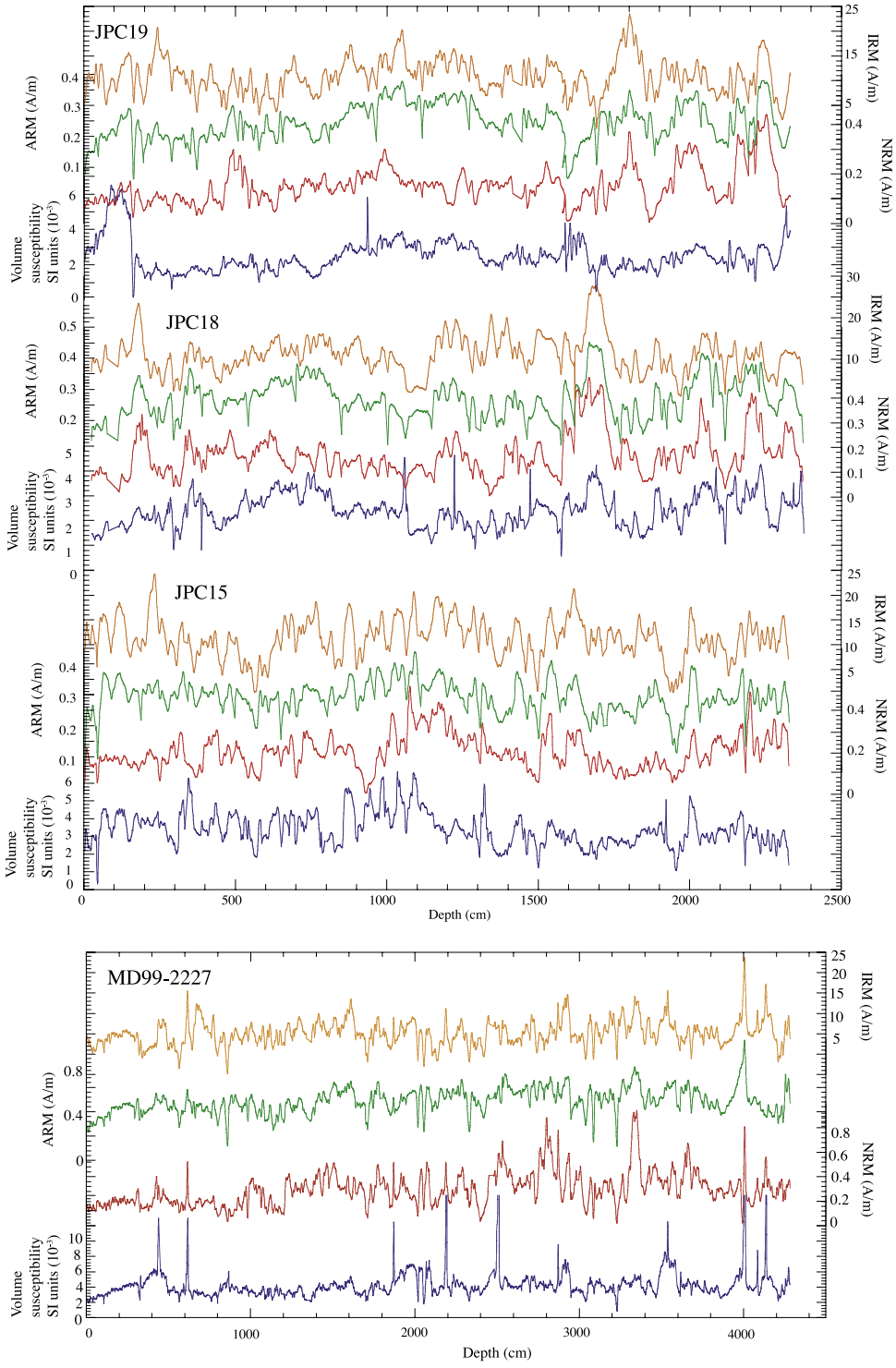

Figure 5. NRM, ARM, and IRM intensities and volume susceptibility for Cores MD99-2227, JPC15, JPC18, and JPC19. Orange, IRM; green, ARM; red, NRM; blue, volume susceptibility.

were analyzed in the stable isotope laboratory at Rutgers University. For all the cores, foraminifer shells of the planktonic species *Neogloboquadrina pachyderma* (left coiling) were picked from the 150–250 μm grain-size fraction for the isotopic analyses. Planktonic foraminifer species were used for the isotopic analyses due to the small amount of benthos present in the cores. For Core MD99-2227, samples were collected at 5 cm intervals for carbonate analyses using an elemental analyzer.

[16] Age models for the piston cores were constructed by matching relative geomagnetic paleointensity records and planktic $\delta^{18}O$ records to target curves, using the location of magnetic excursions (Laschamp and Iceland Basin) to provide additional age constraints. The combination of paleointensity records and oxygen isotope data provide enhanced temporal resolution compared to using either data set independently.

4. NRM and Normalized Remanence Record

[17] The natural remanent magnetization (NRM) data for all four cores are shown as component inclination, corrected component declination, and maximum angular deviation (MAD) values (Figure 2). Orthogonal projections of NRM demagnetization data indicate a single magnetization component (Figure 3b) with no evidence for a high coercivity remanence carrier. Magnetic excursions were identified in three cores from 8-cm^{-3} and 1-cm^{-3} discrete samples as well as from u-channel samples (Figure 3a). U-channel data were deconvolved for comparison with the discrete sample data using the technique of *Oda and Shibuya* [1996], modified for application to u-channel data by *Guyodo et al.* [2002].

[18] Cores were not oriented during collection, and therefore declination data were corrected by aligning the mean declination of each core to North. Twisting within cores during the coring process is indicated by anomalous declination changes in Core JPC18 (114.5–189 cm interval) (Figure 2). Core MD99-2227 is affected by stretching in the upper 15 m that has significantly affected the magnetization directions (Figure 2). Stretching in this interval is also implied by anisotropy of magnetic susceptibility (AMS) measurements carried out shipboard [see *Turon et al.*, 1999].

[19] It is generally accepted that the generation of useful paleointensity proxies requires that the sediments contain magnetite as the only magnetic remanence carrier, have a narrow range of magnetite concentration, as indicated by magnetic concentration parameters varying by less than an order of magnitude, and have restricted magnetite grain-sizes in the few micron grain-size range, corresponding to pseudo-single domain (PSD) grains [*Banerjee*, 1981; *King et al.*, 1982; *Tauxe*, 1993]. There is no evidence from demagnetization characteristics of NRM (Figure 3b), or from hysteresis parameters, for the presence of high-coercivity magnetic minerals such as hematite or pyrrhotite. Using plots of anhysteretic susceptibility against susceptibility, and the calibration of *King et al.* [1982, 1983], we estimate that these sediments generally have mean magnetite grain sizes of $\sim$5 μm (Figure 4). Records of ARM, IRM and susceptibility (Figure 5) show that the concentration parameters generally vary within one order of magnitude, the limit deemed suitable for determination of relative paleointensity proxies [*Tauxe*, 1993]. For coarser-grained intervals in the early part of interglacial stages and in centimeter-scale detrital layers (blue circles and red squares in Figure 4a), relative paleointensity determinations are likely to be less reliable; however, we do not see any marked perturbations associated with these layers. Although these intervals are coarser grained they still fall within the pseudo-single domain (PSD) grain size in the hysteresis ratio plot of *Day et al.* [1977] (Figure 4b).

[20] NRM measured on u-channel samples was normalized using both ARM and IRM, demagnetized at the same peak fields as the NRM. To generate the paleointensity proxies, a mean of nine demagnetization steps in the 20–60 mT peak field interval were used to calculate mean NRM/ARM and mean NRM/IRM. Although the two proxies are generally consistent with each other, mean NRM/ARM has the lower standard deviations over the 20–60 mT demagnetization interval and was therefore chosen as the preferred paleointensity proxy. Coherence analysis for each core, using the Analyseries software of *Paillard et al.* [1996], indicates that the preferred paleointensity proxy (NRM/ARM) and the normalizer (ARM) are not significantly coherent at the 95% confidence level, implying that the paleointensity proxies are not controlled by the ARM concentration (lithologic) parameter.

5. Chronology

[21] To construct age models for the four cores in this study (Figures 6–9), we correlate prominent features (mainly terminations) in the planktonic oxygen isotope records to the benthic oxygen

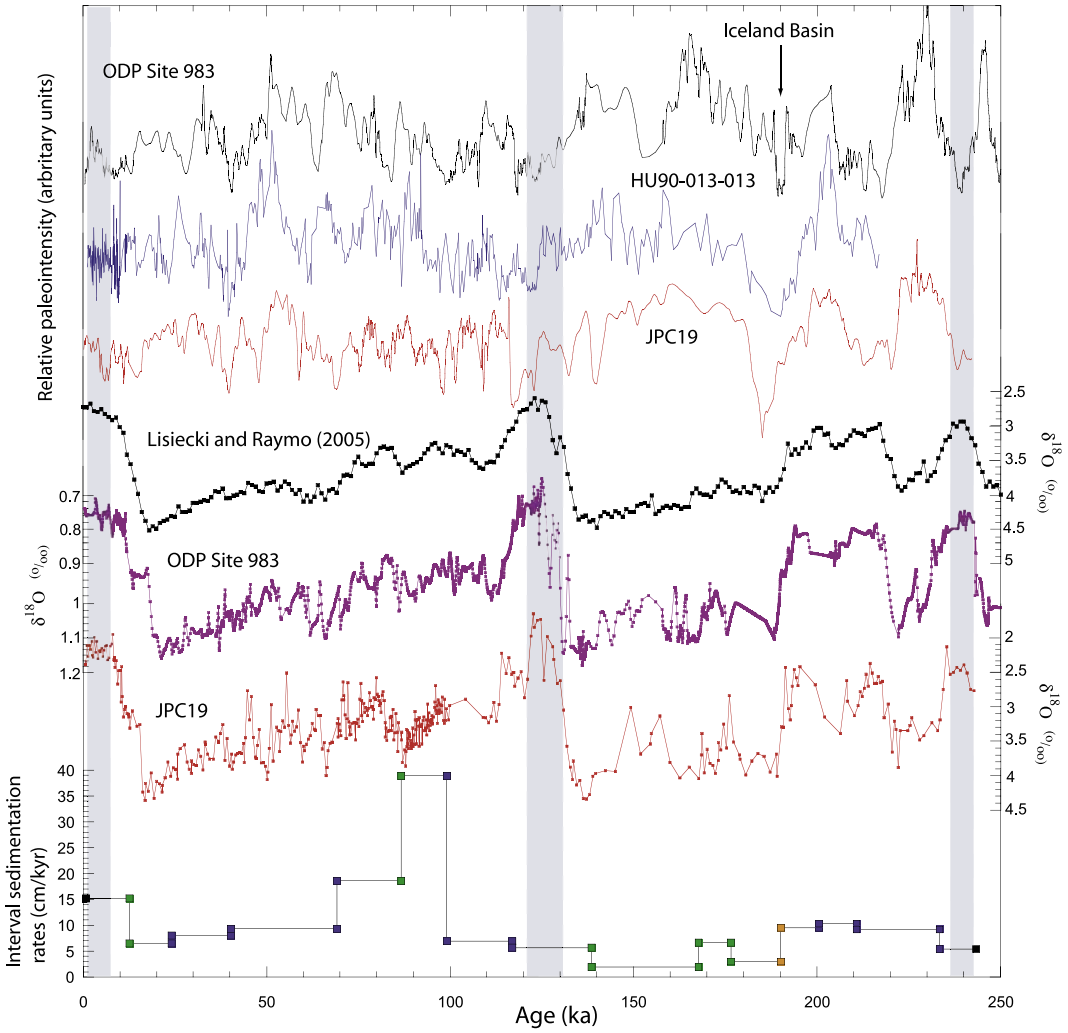

Figure 6. Core JPC19: Relative paleointensity record correlated to the records from ODP Site 983 [*Channell et al.*, 1997]. The relative paleointensity record from Core HU90-013-013 is shown for comparison [*Stoner et al.*, 1995a]. Bottom plots show planktic δ^{18}O data from JPC19 correlated to the benthic δ^{18}O stack of *Lisiecki and Raymo* [2005]. The benthic oxygen isotope record from ODP Site 983 is shown for comparison [*Channell et al.*, 1997]. Shaded areas indicate intervals of coarser magnetic grain sizes associated with deglaciations and interglacials. Interval sedimentation rates are shown with blue squares indicating paleointensity tie-points, green squares indicating isotope tie-points, and orange squares indicating tie-points from directional excursions.

isotope stack of *Lisiecki and Raymo* [2005]. We then correlated the relative paleointensity records to the paleointensity record from ODP Site 983 [*Channell et al.*, 1997; *Channell*, 1999]. The paleointensity record from Core HU90-013-13 [*Stoner et al.*, 1995a] is shown in Figures 6–9 for comparison. Following *Stoner et al.* [2003], the paleointensity and oxygen isotope data from ODP Site 1089 were used to improve the age model for ODP Site 983. For the Eirik Drift cores, a combination of oxygen isotope and relative paleointensity data results in a higher-resolution age model than would be possible using either data set independently. The positions of the tie points that rely on the isotopic data (green), paleointensity data (blue) and directional excursions (orange) are indicated on the sedimentation rate plot (Figures 6–9 and Table 3).

[22] The magnetic excursion recorded at 18.7 mbsf in Core JPC19 (Figures 2 and 3) is interpreted as the Iceland Basin excursion [*Channell et al.*, 1997; *Channell*, 1999]. It lies in a prominent paleointensity low at 185 ka (Figure 6) where the oxygen isotope data are consistent with the transition from MIS 7 to 6. According to the age model (Figure 6), Core JPC19, from the crest of the drift at a water depth of 3184 m, has an age at its base of 245 ka with a mean sedimentation rate of 10.5 cm/ka.

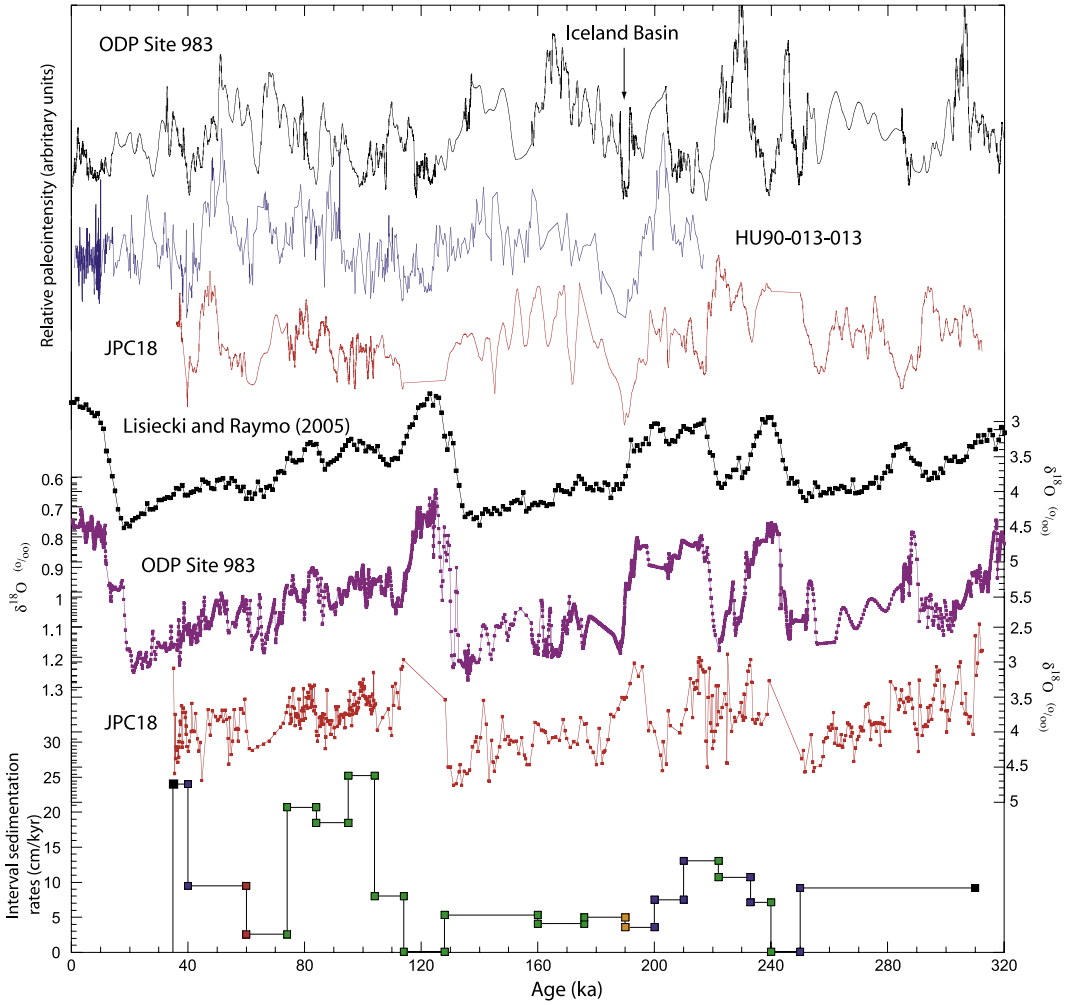

Figure 7. Core JPC18: Relative paleointensity data correlated to ODP Site 983 [*Channell et al.*, 1997]. The relative paleointensity record from HU90-013-013 is shown for comparison [*Stoner et al.*, 1995a]. Bottom plots show planktic δ^{18}O data from JPC18 correlated to the benthic δ^{18}O stack of *Lisiecki and Raymo* [2005]. The benthic oxygen isotope record from ODP Site 983 is shown for comparison [*Channell et al.*, 1997]. Interval sedimentation rates are shown in black (color coding for interval sedimentation rate changes as for Figure 6 with red squares indicating tie-points from both isotope data and paleointensity data).

[23] In Core JPC18, from southern flank of the Eirik ridge at a water depth of 3435 m, sediments coeval with interglacial periods are apparently missing as shown by the lack of oxygen isotope values consistent with the Holocene or MIS 5e (Figure 7). The polarity excursion observed at 13.45 mbsf (Figures 2 and 3) is coeval with the Iceland Basin excursion (Figure 7). The mean sedimentation rate in Core JPC18 is 9 cm/ka and the core has an age of 310 ka at its base.

[24] Core JPC15 was taken on the upper slope of Eirik ridge at a water depth of 2230 m. The polarity excursion observed at 9.3 mbsf in JPC15 (Figures 2 and 3) occurs within a prominent paleointensity low at ~40 ka (Figure 8) and is therefore interpreted as the Laschamp excursion. The base of JPC15 has an age of 160 ka and the mean sedimentation rate is 15 cm/ka (Figure 8).

[25] Core MD99-2227 shows significant stretching in the upper 15 m of the core; however, correlation to the ODP Site 983 paleointensity record is possible below that level corresponding to ~130 ka (Figure 9). The paleointensity correlation to ODP Site 983 is consistent with the correlation of the planktic oxygen isotope record to the benthic oxygen isotope stack of *Lisiecki and Raymo* [2005]. These correlations give a basal age for MD99-2227 of 430 ka, and a mean sedimentation rate of 10 cm/ka (Figure 9).

[26] Radiocarbon ages are available for the last 15 ka at MD99-2227 [*Fagel et al.*, 2004, Table 1].

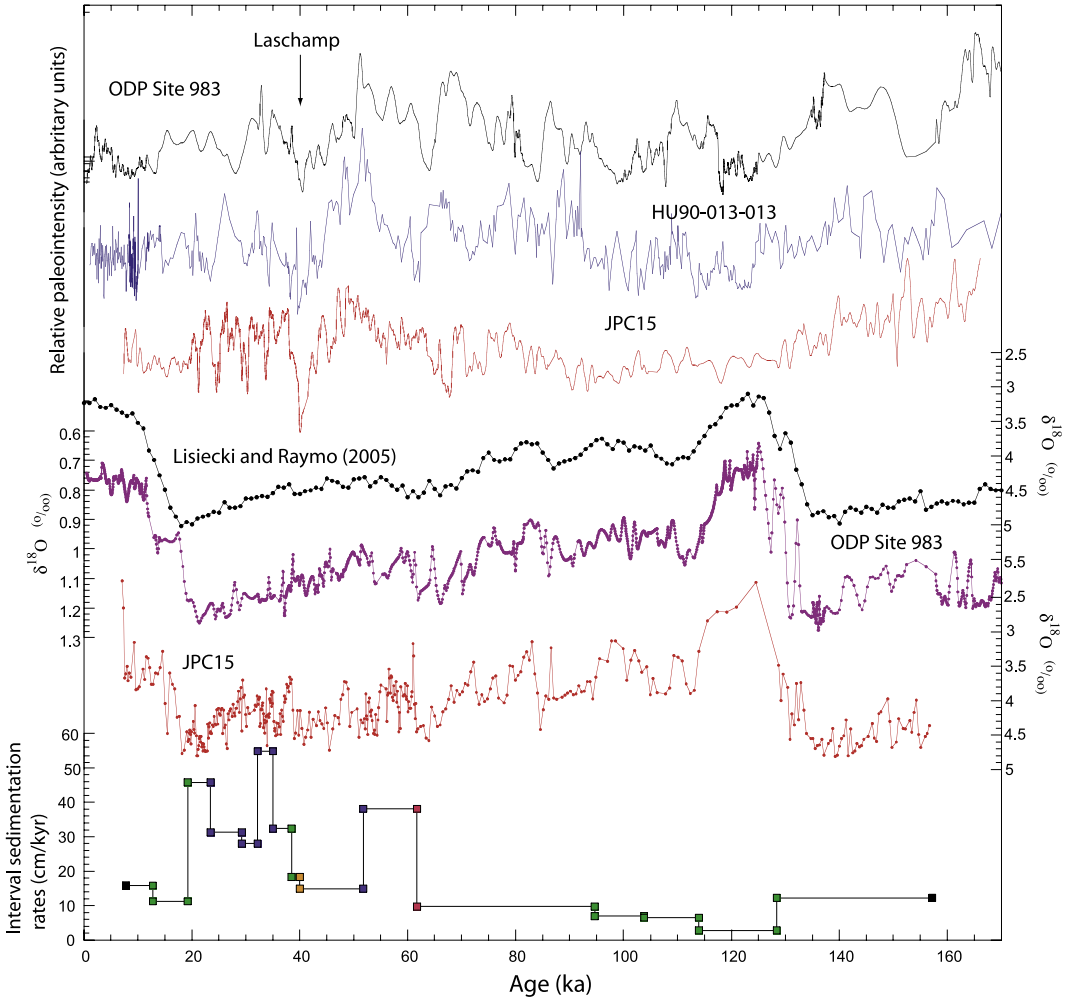

Figure 8. Core JPC15: Relative paleointensity data correlated to ODP Site 983 [*Channell et al.*, 1997]. The relative paleointensity record from HU90-013-013 is shown for comparison [*Stoner et al.*, 1995a]. Bottom plots show planktic $\delta^{18}O$ data from JPC15 correlated to the benthic $\delta^{18}O$ stack of *Lisiecki and Raymo* [2005]. The benthic oxygen isotope record from ODP Site 983 is shown for comparison [*Channell et al.*, 1997]. Interval sedimentation rates are shown in black (color coding as for Figure 7).

These ages are consistent with the age model derived from oxygen isotopes and relative paleointensity data (Figure 9). The radiocarbon ages were measured on monospecific samples of *Neogloboquadrina pachyderma* (left coiled), and converted into calendar years using the radiocarbon calibration program Calib 4.3 [*Fagel et al.*, 2004].

6. Detrital Layer Stratigraphy and Sedimentation Patterns on Eirik Drift

6.1. Decimeter-Scale Detrital Layers

[27] The ratio of anhysteretic susceptibility to susceptibility (k_{arm}/k) has been shown to be a useful magnetite grain size proxy [e.g., *King et al.*, 1983; *Tauxe*, 1993]. Plots of k_{arm} versus k for each core indicate magnetite grain sizes within a restricted (few micron) range, with coarser grains during distinct intervals (Figure 4a). The k_{arm}/k data plotted versus age (Figure 10) indicate distinct broad intervals of low values of k_{arm}/k that coincide with the early Holocene (when recorded), with MIS 5e, and with the early parts of MIS 7, 9 and 11 (shaded in Figure 10). Low values of k_{arm}/k indicate relatively coarse magnetite grain sizes in these intervals. Although Core JPC18 is missing part of the Holocene, and almost the entire MIS 5e, the intervals of low values of k_{arm}/k appear to be partially recorded.

[28] Volume magnetic susceptibility data measured on u-channel samples from JPC19 and MD99-2227 show an increase in magnetic concentration in the early Holocene, MIS 5e, and in MD99-2227 in the

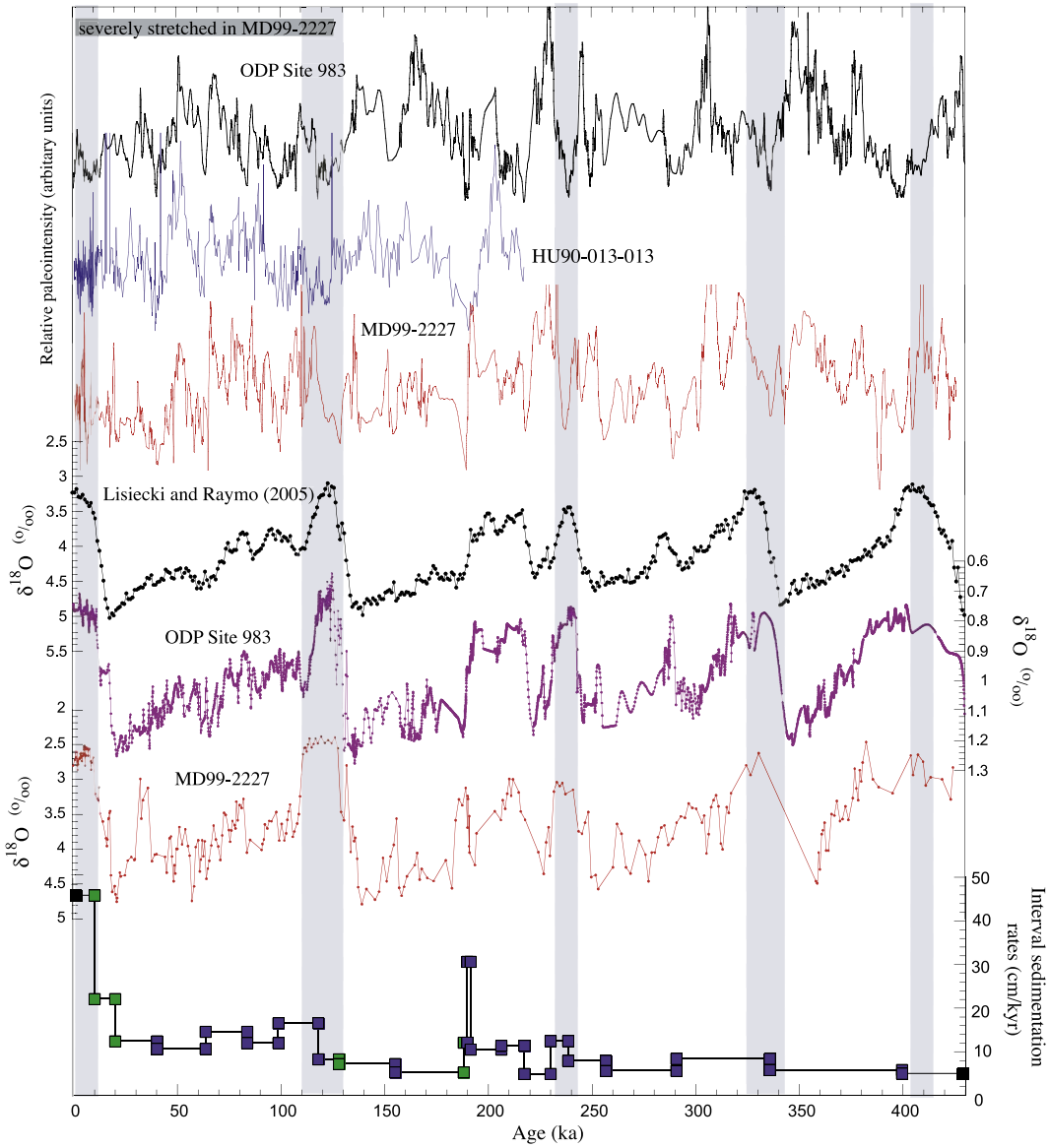

Figure 9. Core MD99-2227: Relative paleointensity data correlated to ODP Site 983 [*Channell et al.*, 1997; *Channell*, 1999]. The relative paleointensity record from HU90-013-013 is shown for comparison [*Stoner et al.*, 1995a]. Bottom plots show planktic δ^{18}O data from MD99-2227 correlated to the benthic δ^{18}O stack of *Lisiecki and Raymo* [2005]. The benthic oxygen isotope record from ODP Site 983 is shown for comparison [*Channell et al.*, 1997]. Black bar (at top left) indicates stretched interval due to coring-related deformation. Shaded areas indicate intervals of coarser magnetic grain sizes associated with deglaciations and interglacials. Interval sedimentation rates are shown in black (color coding as for Figure 7).

early parts of MIS 7, 9 and 11 (Figure 10). These intervals of high magnetic concentration coincide with the intervals of low values of k_{arm}/k (Figure 10) that indicate relatively coarse magnetite grain sizes.

6.2. DC and LDC Centimeter-Scale Detrital Layers

[29] In addition to the broad decimeter-scale intervals defined by k_{arm}/k and k values in Core MD99-2227, a total of seventeen centimeter-scale layers with magnetic properties and percent carbonate values significantly different from the surrounding sediments were observed (Figure 11). These layers have been labeled as either detrital (non-biogenic) carbonate (DC) or low detrital carbonate (LDC) layers, and numbered according to the marine isotope stage in which they are found. For example, 6LDC indicates a low detrital carbonate (LDC) layer within MIS 6 (see Table 2).

Table 3. Age-Depth Tie-Points Used in the Construction of the Age Models for Cores JPC15, JPC18, JPC19, and MD99-2227

Depth, cm	Age, ka	Tie-Point
	JPC15	
7.5	7	top of core
102	12	end Termination I
175	19	Termination I
371	23	paleointensity low
552	29	paleointensity low
633	32	paleointensity high
759	35	paleointensity high
901	38	Isotope 3/4
929	40	Laschamp Excursion
1104	51	paleointensity high
1483	61	Isotope 4/5
1802	95	Isotope 5b/5c
1866	104	Isotope 5c/5d
1932	114	Isotope 5d/5e
1973	128	Isotope 5/6
2324	157	base of core
	JPC18	
0	35	top of core
120	40	Laschamp PI low
310	60	Isotope 3/4, PI Low
346	74	Isotope 4/5a
553	84	Isotope 5a/5b
756	95	Isotope 5b/5c
983	104	Isotope 5c/5d
1063	114	Isotope 5d/5e
1064	128	Isotope 5/6
1235	160	Isotope 6/7
1300	176	Isotope 7.1/7.2
1350	190	Iceland Basin Excursion
1400	200	paleointensity high
1475	210	paleointensity low
1632	222	Isotope stage 7
1750	233	paleointensity low
1800	240	Isotope 7/8
1801	250	paleointensity low
2352	310	base of core
	JPC19	
5.5	0.8	top of core
185	12	Termination I
259	24	PI low
389	40	Laschamp PI low
658	69	PI low
983	86	Isotope 5a/5b
1467	99	PI low
1590	116	PI low
1712	138	Isotope T II
1767	167	Isotope 6/7
1825	176	Isotope 7.1/7.2
1866	190	Iceland Basin Excursion
1966	200	PI high
2071	210	PI low
2278	233	PI low
2332	243	base of core
	MD99-2227	
9	1.1	top of core
417	12	End Termination I
638	20	Termination I
889	40	Laschamp PI Low
1138	63	PI low
1430	83	PI low
1611	98	PI low
1930	118	PI low
2013	128	Isotope 5/6
2208	155	PI low
2382	188	Isotope
2405	189	Iceland Basin PI low
2451	191	Iceland Basin PI low
2607	206	PI low
2734	217	PI low
2796	230	PI high
2902	238	PI low
3047	256	PI low
3238	290	PI low
3617	335	PI low
3990	399	PI low
4136	428	base of core

[30] Eight of the seventeen centimeter-scale layers are designated detrital carbonate layers (DC) on the basis of their high detrital carbonate contents. Four of these layers (3DC, 7DCa, 8DC, 11DC) are recognized by coarser grained magnetic material (compared to the background sediment), as indicated by low k_{arm}/k values (Figure 11). One of these DC layers (7DCa) shows a peak in magnetic susceptibility while the other seven DC layers do not. Two DC layers (5DC, 9DC) show finer-grained magnetite (compared to background sediment), and two DC layers (7DCb, 2DC) are not differentiated by magnetic grain size from the background sediment. All DC layers coincide with highs in percent carbonate and six show peaks in bulk (GRA) density (Figure 11). All DC layers are light in color, do not show a sharp base, and appear to show some bioturbation. The X-radiographs of these layers confirm a high concentration of IRD, but no laminae or evidence for traction (Figure 12). Smear slides indicate a high percentage of coarse detrital carbonate material in these layers, and three of these layers (11DC, 8DC and 7DCa) have high percentages of material in the >106 μm fraction measured at 1–10 cm sample spacing (Table 2).

[31] Nine of the seventeen centimeter-scale detrital layers are designated low detrital carbonate (LDC) layers (Figure 11). These do not feature an increase in percent carbonate, but show a peak in magnetic susceptibility, a low in k_{arm}/k, and an increase in bulk (GRA) density. These LDC layers occur within MIS 1, 2, 5, 6, 7, 9 and 11 and show sharp bases, bioturbated tops and are 4 to 18 cm thick

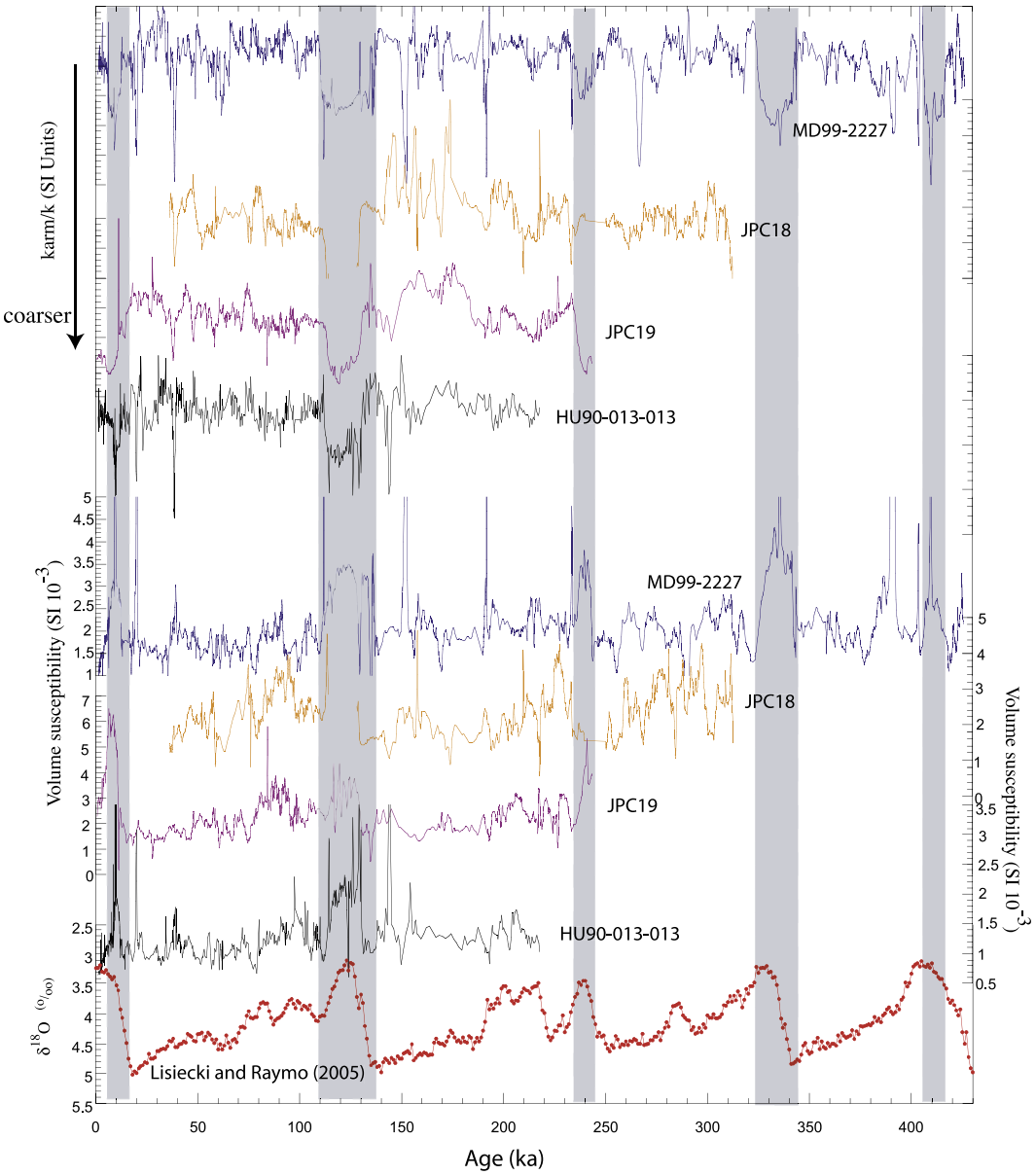

Figure 10. k_{arm}/k and magnetic susceptibility versus age for Cores JPC19, JPC18, and MD99-2227 compared to Core HU90-013-013 [*Stoner et al.*, 1995a]. The benthic oxygen isotope stack of *Lisiecki and Raymo* [2005] is shown at the base of the figure. Shaded areas indicate magnetic coarse grain-size intervals (from k_{arm}/k) and higher magnetic concentration intervals (from susceptibility) in early and peak interglacial intervals.

(Figure 11, Table 2). The X-radiographs indicate a sharp base and laminae within the layers (Figure 12), some of the laminae are inclined and indicative of traction, implying rapid deposition from turbidity currents or contourites.

[32] Toothpick-sized samples collected at 1-cm intervals through detrital layers were used to determine magnetic hysteresis parameters that can be used as a means of assessing the grain size of magnetite [*Day et al.*, 1977]. All but one of the detrital layers exhibit hysteresis parameters that fall within the pseudo-single domain (PSD) grain size range (Figure 13). The detrital carbonate layer identified in MIS2 (2DC) shows coarse multidomain magnetite that is anomalous compared to all other detrital layers (Figure 13). For five of the nine LDC layers, we see evidence for progressive change in hysteresis parameters through the detrital layer indicative of grading, fining upward from the base of the layer. Bioturbation of the detrital layer into the overlying sediment could also cause the

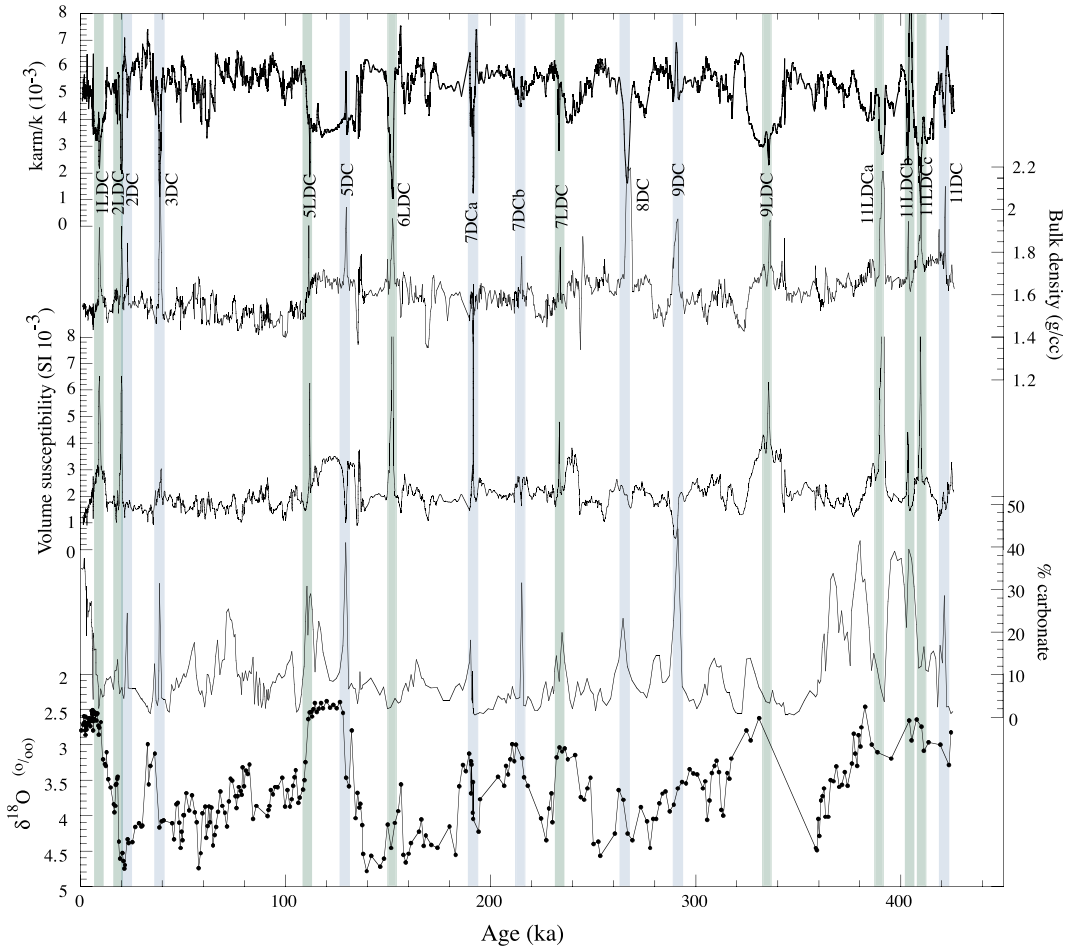

Figure 11. Core MD99-2227: k_{arm}/k, magnetic susceptibility, bulk (GRA) density, percent carbonate, and planktic oxygen isotope data. Blue shading indicates detrital carbonate (DC) layers, and green shading indicates low detrital carbonate (LDC) layers. Bulk density from *Turon et al.* [1999].

layer to appear graded; however, the presence of distinct laminae within the LDC layers suggests that this is not the case. None of the DC layers show "grading" of the hysteresis parameters, suggesting that the depositional process and source of these layers is distinct. We contend that the presence of grading in the LDC layers indicates a turbiditic rather than a contourite origin for these layers.

[33] Smear slides indicate that LDC layers contain little clay and significant amounts of silt-sized opaque grains, green hornblende and quartz. Trace amounts of detrital carbonate are present in LDC layers and throughout the rest of the core, whereas the percentage of detrital carbonate in the DC layers exceeds 10% (Table 2).

6.3. Sedimentation Patterns on Eirik Drift

[34] Sedimentation rates on the Eirik Drift have been shown to be greatly affected by changes in the strength and bathymetry of the Western Boundary Undercurrent (WBUC) that is thought to be switched off during glacial stages and active during interglacials [*Hillaire-Marcel et al.*, 1994; *Hillaire-Marcel and Bilodeau*, 2000]. The core of this current is thought to occupy water depths between 2500 and 3000 m [*Hillaire-Marcel et al.*, 1994], resulting in winnowing and almost completely removal of Holocene and MIS 5e sediment from these depths. Cores from outside the influence of the flow would be expected to have interglacial sedimentation rates comparable to, or higher than, glacial sedimentation rates.

[35] When combined with previous studies carried out on the drift, the new results indicate that both water depth and position on the drift influence sediment accumulation rates. Although the site of Core JPC18 is located ~450 m below the supposed core of the WBUC, sediment of Holocene and MIS 5e age is missing at this site. This implies that the

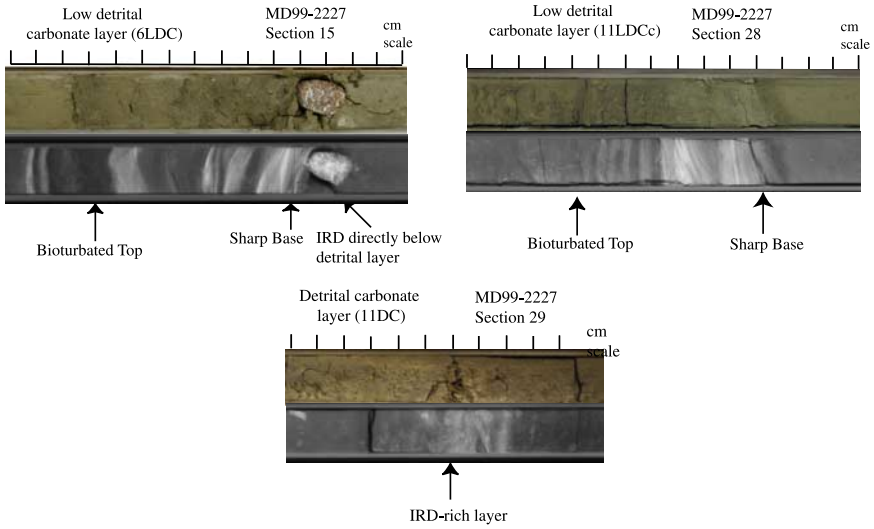

Figure 12. Photographs (top portion) and X-radiographs (bottom portion) of three detrital layers identified in Core MD99-2227. MD99-2227 section 15 (6LDC), MD99-2227 section 28 (11LDCc), and MD99-2227 section 29 (11DC). In X-radiographs, lighter shades indicate higher density, and darker shades indicate lower density.

WBUC is active at deeper water depths than previously supposed on the southern side of the Eirik ridge (Figure 1). This may be consistent with a deep branch of the WBUC within a gyre that feeds the Gloria Drift (Figure 1).

[36] Core HU90-013-013 (water depth 3471 m), Core JPC19 (water depth 3184 m) and Core MD99-2227 (water depth 3460 m) have relatively high Holocene sedimentation rates of 35 cm/ka, ~13 cm/ka, and 10 cm/ka, respectively. Core HU90-013-012 at 2830 m water depth lies within the influence of the WBUC and has very low sedimentation rates in the Holocene [*Stoner et al.*, 1995a, 1998]. Higher up the slope, Core JPC15 at a water depth of 2230 m has low sedimentation rates in the Holocene and MIS 5e, although the site supposedly lies outside the main influence of the WBUC. *Hillaire-Marcel et al.* [1994] noted that, in core HU90-013-06 at even shallower water depths (1105 m) on the Eirik ridge, active bottom currents also resulted in very low Holocene sedimentation rates.

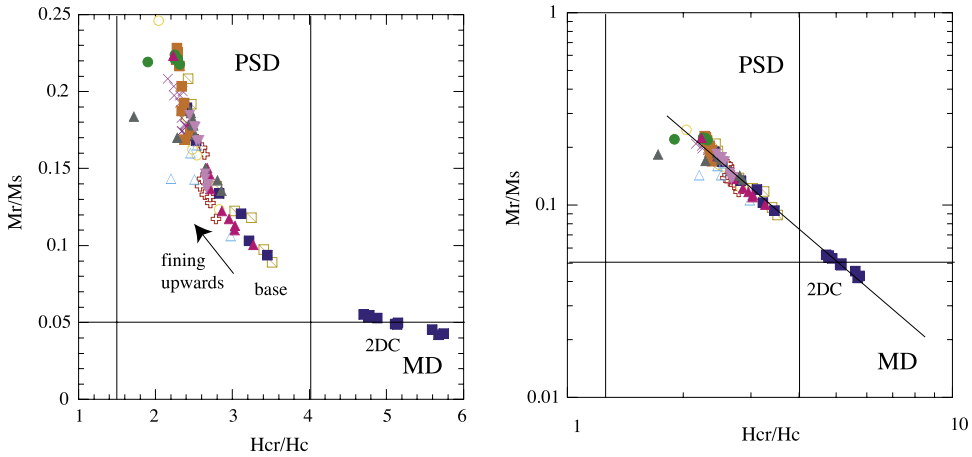

Figure 13. (left) Hysteresis ratio Mr/Ms plotted versus Hcr/Hc for individual centimeter-scale detrital layers from Core MD99-2227 shown by colored symbols. Pseudo-single domain (PSD) and multidomain (MD) fields after *Day et al.* [1977]. Five out of nine show fining upward as indicated by arrow. Detrital carbonate layer 2DC (coeval with H2) has anomalously coarse magnetite grain size but no apparent grading. (right) Hysteresis ratios Mr/Ms plotted versus Hcr/Hc on a log-log scale, with sample data lying on a magnetite mixing line.

6.4. Correlations Among North Atlantic Detrital Layers

[37] The centimeter-scale detrital layers identified in Core MD99-2227 extend the record of detrital layers beyond the last glacial cycle. Detrital layers on Eirik Drift occur during both glacial and interglacial conditions; however, the layers occurring in the interglacials are close to the onset of the isotopic stages for the Holocene, MIS 5, 7 and 11. It is only in MIS 9 that a DC layer appears to occur in the later part of the interglacial implying that the Laurentide Ice Sheet existed throughout MIS 9.

[38] Detrital layer 1LDC with an age of 9.12 ka in MD99-2227 (Table 4) is tentatively correlated to a k_{arm}/k peak in HU90-013-013 [see *Stoner et al.*, 1995b, Figure 3]. Layer 2LDC has an age of 20.2 ka and is correlated to the event labeled Me1 (~17 ka) in HU90-013-013 [*Stoner et al.*, 1995b] and to the "b" layer of *Bond and Lotti* [1995]. The layer 2DC correlates with DC2 of *Stoner et al.* [1998] and with H2 [*Bond et al.*, 1999]. The detrital layer labeled 3DC (39 ka) is correlated to DC4 from Orphan Knoll and to H4 (38 ka). As discussed above, the characteristics of LDC layers implies deposition by turbidity currents (derived from the Greenland Slope). If so, this turbiditic activity is sometimes coeval with Heinrich layers of the central Atlantic and with detrital events at Orphan Knoll.

[39] On the East Greenland margin, *Elliot et al.* [1998] identified all six Heinrich layers and thirteen other subsidiary detrital layers in the 10–60 ka interval in Core SU90-24 from the Irminger Basin. Three detrital layers identified in this core apparently correlate with detrital layers identified in MD99-2227 (Table 4). H2 is apparently correlative between the two cores, and detrital layers DEc (19 ka) and DE (40 ka) in Core SU90-24 correlate to a 2LDC and 3DC, respectively, in Core MD99-2227. The ages of layers designated 2DC and 3DC in this study are consistent with ages for Heinrich events H2, and H4 (Table 4). No detrital events coeval with Heinrich events H1, H3, H5 or H6 are observed in cores from Eirik Drift.

[40] *Hiscott et al.* [2001] identified Heinrich-like detrital layers in Core MD95-2025 from near Orphan Knoll (Figure 1) back to MIS 9. Two detrital carbonate layers in early MIS 5 at Orphan Knoll (H8 and H9 of *Hiscott et al.* [2001]) appear to be coeval with DC events identified on Eirik Drift, implying that instabilities of the Laurentide Ice Sheet are recorded at both sites. Detrital carbonate layers within MIS 7 and MIS 9 at Orphan Knoll (H10 and H13 of *Hiscott et al.* [2001]) appear to be coeval with a LDC layers (7LDC and 10 LDC) identified on Eirik Drift (Table 4), implying that the LIS instabilities that triggered the detrital carbonate layers at Orphan Knoll were coeval with instabilities on the Greenland slope that triggered the LDC layers on Eirik Drift. Such conclusions are highly dependent on the resolution of stratigraphic correlation. While stratigraphic correlation of detrital layers from the Orphan Knoll to the central Atlantic for the last glacial cycle is rather well constrained [*Bond et al.*, 1999; *Stoner et al.*, 1996, 2000], the correlations beyond the last glacial cycle are considerably more speculative [*Hiscott et al.*, 2001; *van Kreveld et al.*, 1996] due to lack of stratigraphic resolution that inhibits unequivocal correlation of detrital layers.

7. Conclusions

[41] Four piston cores collected from Eirik Drift have produced records of decimeter and centimeter-scale detrital layers that appear to reflect episodes of instability in surrounding ice sheets. We place these detrital layers into a chronostratigraphic framework based on relative paleointensity proxies and oxygen isotope data, with additional age constraints provided by recognition of two magnetic excursions (Laschamp and Iceland Basin).

[42] Magnetic data from Cores JPC19 and MD99-2227 show broad intervals of increased magnetite grain size and concentration during MIS 5e and at the MIS 2/1 transition, consistent with observations from Core HU90-013-013 [*Stoner et al.*, 1995b]. Core MD99-2227 also shows a similar increase in magnetite grain size and concentration at the onset of interglacial MIS 7, 9 and 11, implying that retreat of the Greenland Ice Sheet produced a characteristic detrital signal at the onset of all interglacial stages over the last 400 ka.

[43] Seventeen centimeter-scale detrital carbonate and low detrital carbonate layers are identified in MD99-2227 (Figure 11 and Table 2). They occur in both glacial and interglacial stages. The detrital layers can be subdivided into two classes. Detrital carbonate (DC) layers are composed of carbonate-rich IRD. They usually, but not always, carry a magnetic signal indicating high magnetic concentration and increased magnetite grain size relative to background sediment. Low detrital carbonate (LDC) layers have <10% detrital carbonate, usual-

Table 4. Detrital Layers From Other Studies Correlative to Detrital Layers Identified on Eirik Drift

Event	Name	Depth, cm	MD99-2227, ka	*Stoner et al.* [1995b], ka	*Stoner et al.* [1998], ka	H-layers [*Bond et al.*, 1999], ka	*Hiscott et al.* [2001], ka	*van Kreveld et al.* [1996], ka	*Bond and Lotti* [1995], ka	*Elliot et al.* [1998], ka
1	1LDC	440	9.12	9.1[a]						
2	2LDC	617	20.2	Me1(17)					b(21)	DEc (19)
3	2DC	663	22.8		DC2 (23.5)	H2 (24)	H2 (18–22)	h2 (21)		He2 (20–22)
4	3DC	859	39.1		DC4 (36)	H4 (38)	H4 (39–42)	h4 (40–43)	H4 (39)	DE (40)
5	5LDC	1872	111.7				H8(92–108)			
6	5DC	2019	129.3				H9(121–126)	h7 (128–131)		
7	6LDC	2193	152.2							
8	7DCa	2505	191.6					h12 (189)		
9	7DCb	2700	215							
10	7LDC	2872	233.4				H10(231–240)			
11	8DC	3084	266.6							
12	9DC	3229	290							
13	9LDC	3536	335.6				H13(335–340)			
14	11LDCa	4008	391							
15	11LDCb	4084	403.5							
16	11LDCc	4134	409.6							
17	11DC	4240	421.4							

[a] The karm/k low identified in Core HU90-013-013 by *Stoner et al.* [1995b] but not named [see *Stoner et al.*, 1995b, Figure 3].

ly show evidence (from magnetic hysteresis ratios) for fining-upward grading, and X-radiograph evidence for traction. These layers are also usually marked by high magnetic concentration and increased magnetite grain size relative to background sediment.

[44] On the basis of the differences between DC and LDC layers, we interpret the former as Hudson Strait derived detrital layers, and the latter as layers dominated by material from turbidites derived from the Greenland slope. 1LDC, 2LDC, 2DC and 3DC are correlative with detrital layers observed at Orphan Knoll [*Stoner et al.*, 1996] (Table 4). Two of them (2DC and 3DC) are coeval with central Atlantic Heinrich layers H2 and H4 [*Bond et al.*, 1999]. Beyond the last glacial cycle, the correlation of detrital layers from Eirik Drift (this paper) to Orphan Knoll [*Hiscott et al.*, 2001] and to the central Atlantic [*van Kreveld et al.*, 1996] is limited by imprecision of stratigraphic correlation (Table 4). Nonetheless, as illustrated here, the use of paleointensity-assisted chronostratigraphy, the combination of relative paleointensity with standard oxygen isotope stratigraphy, improves stratigraphic correlations across the northern North Atlantic Ocean (and beyond), and thereby facilitates the interpretation of detrital layers in terms of their correlation, aerial extent and provenance.

Acknowledgments

[45] We acknowledge the IMAGES program for the recovery of Core MD99-2227 and NSF for support of cruise KN166-14 of the R/V *Knorr*. This research was supported by NSF grant OCE-0350830 to Channell and by CFCAS and NSERC grants to Hillaire-Marcel. We thank John Jaeger and Gillian Rosen for facilitating and interpreting the X-radiographs.

References

Aksu, A. E., A. de Vernal, and P. J. Mudie (1989), High-resolution foraminifer, palynologic and stable isotopic records of Upper Pleistocene sediments from the Labrador Sea: Paleoclimatic and paleoceanographic trends, *Proc. Ocean Drill. Program Sci. Results*, *105*, 617–652.

Alley, R. B., and D. R. MacAyeal (1994), Ice-rafted debris associated with binge purge oscillations of the Laurentide ice sheet, *Paleoceanography*, *9*(4), 503–511.

Andrews, J. T., and K. Tedesco (1992), Detrital carbonate-rich sediments, northwestern Labrador Sea: Implications for ice-sheet dynamics and iceberg rafting (Heinrich) events in the North Atlantic, *Geology*, *20*(12), 1087–1090.

Arthur, M. A., S. P. Srivastava, M. Kaminski, R. Jarrad, and J. Osler (1989), Seismic stratigraphy and history of Deep Circulation and Sediment Drift Development in Baffin Bay and the Labrador Sea, *Proc. Ocean Drill. Program Sci. Results*, *105*, 957–988.

Banerjee, S. K. (1981), Experimental methods of rock magnetism and paleomagnetism, *Adv. Geophys.*, *23*, 25–99.

Bond, G., et al. (1992), Evidence for massive discharges of icebergs into the North Atlantic Ocean during the last glacial period, *Nature*, *360*, 245–249.

Bond, G., W. Broecker, S. Johnsen, J. McManus, L. Labeyrie, J. Jouzel, and G. Bonani (1993), Correlations between climate records from North Atlantic sediments and Greenland ice, *Nature*, *365*, 143–147.

Bond, G. C., and R. Lotti (1995), Iceberg discharges into the North Atlantic on millennial time scales during the last glaciation, *Science*, *267*, 1005–1010.

Bond, G. C., W. Showers, M. Elliot, M. Evans, R. Lotti, I. Hajdas, G. Bonani, and S. Johnson (1999), The North Atlantic's 1–2 kyr climate rhythm: Relation to Heinrich events, Dansgaard/Oeschger cycles and the Little Ice Age, in *Mechanisms of Global Climate Change at Millennial Time Scales*, *Geophys. Monogr. Ser.*, vol. 112, edited by P. U. Clark, R. S. Webb, and L. D. Keigwin, pp. 35–58, AGU, Washington, D. C.

Broecker, W. S., G. C. Bond, M. Klas, E. Clark, and J. F. McManus (1992), Origin of the northern Atlantic's Heinrich events, *Clim. Dyn.*, *6*, 265–273.

Channell, J. E. T. (1999), Geomagnetic paleointensity and directional secular variation at Ocean Drilling Program (ODP) Site 984 (Bjorn Drift) since 500 ka: Comparisons with ODP Site 983 (Gardar Drift), *J. Geophys. Res.*, *104*, 22,937–22,951.

Channell, J. E. T., D. A. Hodell, and B. Lehman (1997), Relative geomagnetic paleointensity and δ^{18}O at ODP Site 983 (Gardar Drift, North Atlantic) since 350 ka, *Earth Planet. Sci. Lett.*, *153*, 103–118.

Channell, J. E. T., J. S. Stoner, D. A. Hodell, and C. D. Charles (2000), Geomagnetic paleointensity for the last 100 kyr from the subantarctic South Atlantic: A tool for inter-hemispheric correlation, *Earth Planet. Sci. Lett.*, *175*, 145–160.

Chough, S. K., and R. Hesse (1985), Contourites from Eirik Ridge, south of Greenland, *Sediment. Geol.*, *41*, 185–199.

Day, R., M. Fuller, and V. A. Schmidt (1977), Hysteresis properties of titanomagnetites: Grain-size and compositional dependence, *Phys. Earth Planet. Inter.*, *13*, 260–267.

Elliot, M., L. Labeyrie, G. Bond, E. Cortijo, J.-L. Turon, N. Tisnerat, and J.-C. Duplessy (1998), Millennial-scale iceberg discharges in the Irminger Basin during the last glacial period: Relationship with the Heinrich events and environmental settings, *Paleoceanography*, *13*(5), 433–446.

Fagel, N., C. Hillaire-Marcel, M. Humblet, R. Brasseur, D. Weis, and R. Stevenson (2004), Nd and Pb isotope signatures of the clay-size fraction of Labrador Sea sediments during the Holocene: Implications for the inception of the modern deep circulation pattern, *Paleoceanography*, *19*, PA3002, doi:10.1029/2003PA000993.

Grousset, F. E., L. Labeyrie, J. A. Sinko, M. Cremer, G. Bond, J. Duprat, E. Cortijo, and S. Huon (1993), Patterns of ice-rafted detritus in the glacial North Atlantic (40–55°C), *Paleoceanography*, *8*(2), 175–192.

Guyodo, Y., and J. P. Valet (1999), Global changes in geomagnetic intensity during the past 800 thousand years, *Nature*, *399*, 249–252.

Guyodo, Y., J. E. T. Channell, and R. G. Thomas (2002), Deconvolution of u-channel paleomagnetic data near geomagnetic reversals and short events, *Geophys. Res. Lett.*, *29*(17), 1845, doi:10.1029/2002GL014927.

Heinrich, H. (1988), Origin and consequences of cyclic ice rafting in the northeast Atlantic Ocean during the past 130,000 years, *Quat. Res.*, *29*, 142–152.

Hemming, S. R. (2004), Heinrich events: Massive late Pleistocene detritus layers of the North Atlantic and their global climate imprint, *Rev. Geophys.*, *42*, RG1005, doi:10.1029/2003RG000128.

Hesse, R., S. K. Chough, and A. Rakofsky (1987), The northwest Atlantic mid-ocean channel of the Labrador Sea: V. Sedimentology of a giant deep-sea channel, *Can. J. Earth Sci.*, *24*, 1595–1624.

Hillaire-Marcel, C., and G. Bilodeau (2000), Instabilities in the Labrador Sea water mass structure during the last climatic cycle, *Can. J. Earth Sci.*, *37*, 795–809.

Hillaire-Marcel, C., A. De Vernal, G. Bilodeau, and G. Wu (1994), Isotope stratigraphy, sedimentation rates, deep circulation, and carbonate events in the Labrador Sea during the last ~200 ka, *Can. J. Earth Sci.*, *31*, 63–89.

Hiscott, R. N., M. Cremer, and A. E. Aksu (1989), Evidence from sedimentary structures for processes of sediment transport and deposition during post-Miocene time at Sites 645, 646 and 647, Baffin Bay and Labrador Sea, *Proc. Ocean Drill. Program Sci. Results*, *105*, 53–63.

Hiscott, R. N., A. E. Aksu, P. J. Mudie, and D. F. Parsons (2001), A 340,000 year record of ice rafting, paleoclimatic fluctuations, and shelf crossing glacial advances in the southwestern Labrador Sea, *Global Planet. Change*, *28*, 227–240.

Horng, C., A. P. Roberts, and W. Liang (2003), A 2.14-Myr astronomically tuned record of relative geomagnetic paleointensity from the western Philippine Sea, *J. Geophys. Res.*, *108*(B1), 2059, doi:10.1029/2001JB001698.

King, J. W., S. K. Banerjee, J. A. Marvin, and Ö. Özdemir (1982), A comparison of different magnetic methods for determining the relative grain size of magnetite in natural materials: Some results from lake sediments, *Earth Planet. Sci. Lett.*, *59*, 404–419.

King, J. W., S. K. Banerjee, and J. Marvin (1983), A new rock-magnetic approach to selecting sediments for geomagnetic paleointensity studies: Application to paleointensity for the last 4000 years, *J. Geophys. Res.*, *88*, 5911–5921.

Kirschvink, J. L. (1980), The least squares lines and plane analysis of palaeomagnetic data, *Geophys. J. R. Astron. Soc.*, *62*, 699–718.

Laj, C., C. Kissel, A. Mazaud, J. E. T. Channell, and J. Beer (2000), North Atlantic paleointensity stack since 75 ka (NAPIS-75) and the duration of the Laschamp event, *Philos. Trans. R. Soc. London, Ser. A*, *358*, 1009–1025.

Laj, C., C. Kissel, and J. Beer (2004), High resolution global paleointensity stack since 75 kyr (GLOPIS-75) calibrated to absolute values, in *Timescales of the Paleomagnetic Field*, *Geophys. Monogr. Ser.*, vol. 145, edited by J. E. T. Channell et al., pp. 255–265, AGU, Washington, D. C.

Lisiecki, L. E., and M. E. Raymo (2005), A Pliocene-Pleistocene stack of 57 globally distributed benthic $\delta^{18}O$ records, *Paleoceanography*, *20*, PA1003, doi:10.1029/2004PA001071.

Lucotte, M., and C. Hillaire-Marcel (1994), Identification et distribution des grandes masses d'eau dans les mers du Labrador et d'Irminger, *Can. J. Earth Sci.*, *31*, 5–13.

MacAyeal, D. R. (1993), Binge/purge oscillations of the Laurentide ice sheet as a cause of the North Atlantic's Heinrich events, *Paleoceanography*, *8*(6), 775–784.

McCave, I. N., and B. E. Tucholke (1986), Deep current-controlled sedimentation in the western North Atlantic, in *The Geology of North America*, vol. M, *The Western Atlantic Region*, edited by P. R. Vogt and B. E. Tucholke, pp. 451–468, Geol. Soc. of Am., Boulder, Colo.

Oda, H., and H. Shibuya (1996), Deconvolution of long-core paleomagnetic data of Ocean Drilling Program by Akaike's Bayesian Information Criterion minimization, *J. Geophys. Res.*, *101*, 2815–2834.

Paillard, D., L. Labeyrie, and P. Yiou (1996), Macintosh program performs time-series analysis, *Eos Trans. AGU*, *77*, 379.

Peck, V. L., I. R. Hall, R. Zahn, F. Grousset, S. R. Hemming, and J. D. Scourse (2007), The relationship of Heinrich events and their European precursors over the past 60 ka BP: A multi-proxy ice-rafted debris provenance study in the North East Atlantic, *Quat. Sci. Rev.*, *26*, 862–875.

Ruddiman, W. F. (1977), Late Quaternary deposition of ice-rafted sand in the subpolar North Atlantic (lat 40 to 65 N), *Geol. Soc. Am. Bull.*, *88*, 1813–1827.

Scourse, J. D., I. R. Hall, I. N. McCave, J. R. Young, and C. Sugdon (2000), The origin of Heinrich layers: Evidence from H2 for European precursor events, *Earth Planet. Sci. Lett.*, *182*, 187–195.

Snoeckx, H., F. Grousset, M. Revel, and A. Boelaert (1999), European contribution of ice-rafted sand to Heinrich layers H3 and H4, *Mar. Geol.*, *158*, 197–208.

Srivastava, S. P., and C. R. Tapscott (1986), Plate kinematics of the North Atlantic, in *The Geology of North America*, vol. M, *The Western Atlantic Region*, edited by P. R. Vogt and B. E. Tucholke, pp. 589–604, Geol. Soc. of Am., Boulder, Colo.

Stoner, J. S., J. E. T. Channell, and C. Hillaire-Marcel (1995a), Late Pleistocene relative geomagnetic paleointensity from the deep Labrador Sea: Regional and global correlations, *Earth Planet. Sci. Lett.*, *134*, 237–252.

Stoner, J. S., J. E. T. Channell, and C. Hillaire-Marcel (1995b), Magnetic properties of deep-sea sediments off southwest Greenland: Evidence for major differences between the last two deglaciations, *Geology*, *23*, 241–244.

Stoner, J. S., J. E. T. Channell, and C. Hillaire-Marcel (1996), The magnetic signature of rapidly deposited detrital layers from the deep Labrador Sea: Relationship to North Atlantic Heinrich layers, *Paleoceanography*, *11*, 309–325.

Stoner, J. S., J. E. T. Channell, and C. Hillaire-Marcel (1998), A 200 kyr geomagnetic chronostratigraphy for the Labrador Sea: Indirect correlation of the sediment record to SPECMAP, *Earth Planet. Sci. Lett.*, *159*, 165–181.

Stoner, J. S., C. Laj, J. E. T. Channell, and C. Kissel (2000), South Atlantic (SAPIS) and North Atlantic (NAPIS) geomagnetic paleointensity stacks (0–80 ka): Implications for inter-hemispheric correlation, *Quat. Sci. Rev.*, *21*, 1141–1151.

Stoner, J. S., J. E. T. Channell, D. A. Hodell, and C. D. Charles (2003), A (580 kyr paleomagnetic record from the sub-Antarctic South Atlantic (Ocean Drilling Program Site 1089), *J. Geophys. Res.*, *108*(B5), 2244, doi:10.1029/2001JB001390.

Tauxe, L. (1993), Sedimentary records of relative paleointensity of the geomagnetic field: Theory and practice, *Rev. Geophys.*, *31*, 319–354.

Thomas, R. G., Y. Guyodo, and J. E. T. Channell (2003), U channel track for susceptibility measurements, *Geochem. Geophys. Geosyst.*, *4*(6), 1050, doi:10.1029/2002GC000454.

Turon, J.-L., C. Hillaire-Marcel, and Shipboard Participants (1999), IMAGES V mission of the Marion Dufresne. Leg 2, 30 June to 24 July 1999, *Open File 3782*, Geol. Surv. of Can., Ottawa, Canada.

van Kreveld, S., M. Sarnthein, H. Erlenkeuser, P. Grootes, S. Jung, M. J. Nadeau, U. Pflaumann, and A. Voelker (2000), Potential links between surging ice sheets, circulation changes, and the Dansgaard-Oeschger cycles in the Irminger Sea, 60–18 kyr, *Paleoceanography*, *15*(4), 425–442.

van Kreveld, S. A., M. Knappertsbusch, J. Ottens, G. Ganssen, and J. van Hinte (1996), Biogenic carbonate and ice-rafted debris (Heinrich layer) accumulation in deep-sea sediments from a Northeast Atlantic piston core, *Mar. Geol.*, *131*, 21–46.

Walden, J., E. Wadsworth, W. E. N. Austin, C. Peters, J. D. Scourse, and I. R. Hall (2007), Compositional variability of ice-rafted debris in Heinrich layers 1 and 2 on the northwest European continental slope identified by environmental magnetic analyses, *J. Quat. Sci.*, *22*(2), 163–172.

Yamazaki, T. (1999), Relative paleointensity of the geomagnetic field during Brunhes Chron recorded in North Pacific deep-sea sediment cores: Orbital influence?, *Earth Planet. Sci. Lett.*, *169*, 23–35.